IEEE Open Journal of
Industry Applications

Received 8 October 2022; revised 15 January 2023 and 20 February 2023; accepted 7 March 2023. Date of publication 13 March 2023; date of current version 18 April 2023. The review of this article was arranged by Associate Editor Mauro Di Nardo.

Digital Object Identifier 10.1109/OJIA.2023.3256364

Determining the Control Objectives of a Switched Reluctance Machine for Performance Improvement in Generating Mode

AHSAN ZAHID AND BERKER BILGIN (Senior Member, IEEE)

Department of Electrical and Computer Engineering, McMaster University, Hamilton, ON L8S 4L8, Canada

CORRESPONDING AUTHOR: BERKER BILGIN (e-mail: bilginb@mcmaster.ca)

This work was supported by the Natural Sciences and Engineering Research Council of Canada (NSERC).

ABSTRACT This article presents a methodology to determine the control objectives of conduction angle control in generating mode of operation in a switched reluctance machine. First, the performance in motoring mode of control is compared with generating mode for different operating points. Then, the key optimization objectives are established to improve a switched reluctance machine's performance in generating mode. A multiobjective optimizer is used to select the conduction angles. The proposed generating-specific objectives are maximizing source current per torque and minimizing torque ripple. These objectives are then compared with the motoring-specific objectives, such as maximizing average torque and minimizing torque ripple for a wide speed range. Finally, the proposed generating objectives have been validated experimentally using a three-phase 12/8 switched reluctance machine.

INDEX TERMS Conduction angle control, genetic algorithm optimization, switched reluctance generator, switched reluctance motor (SRM).

I. INTRODUCTION

In recent years, there is an incentive to utilize methods of transportation which produce lower emissions and are less dependent on volatile natural resources. From the years 2000 to 2018, greenhouse gas (GHG) emissions from the transportation sector in Canada have risen by 27%. This large increase is attributed to an increase in passenger and freight vehicles [1]. Electrification of the transportation sector can result in the reduction of crude oil supply dependence and reduce GHG emissions into the atmosphere.

Currently, the most common electric motor used as a means of propulsion is the permanent magnet synchronous machine (PMSM). PMSMs have high-energy-dense rare-earth permanent magnets (PMs) to provide an independent source of magnetic flux, which results in high torque density and high efficiency [2]. However, rare-earth PMs have significant supply chain issues [3]. Their price and availability are volatile [4]. The mining and extraction of rare earth metals have impact on environment and human health [5]. Also, the performance of rare-earth PMs is strongly dependent on temperature.

Switched reluctance machine (SRM) is a strong alternative to PMSMs. SRMs are low-cost to manufacture, facilitate simple construction, and are composed of a robust structure. SRMs do not have PMs or conductors on the rotor. Hence, the material footprint and environmental footprint can be greatly reduced. SRMs can provide robust operation at high temperatures and high speed due to the lack of separate rotor excitation [6].

The SRM has been a point of interest in the research and academic community, particularly in the topic of developing control schemes to improve performance in motoring mode by using optimization techniques. Some control strategies, such as single pulse control, conduction angle control, and torque sharing functions have been developed to improve motoring performance such as to maximize the average torque production, minimize torque ripple, and reducing losses. Significant work has been done for SRMs in motoring mode to improve specific performance objectives. In [7] and [8], an adaptive control scheme has been presented for an SRM to control the turn-OFF conduction angle using a finite control set model predictive control to reduce the negative torque

This work is licensed under a Creative Commons Attribution-NonCommercial-NoDerivatives 4.0 License. For more information, see https://creativecommons.org/licenses/by-nc-nd/4.0/

production in motoring mode while reducing torque ripple and copper losses at high-speed operation. In [9], the firefly algorithm is used to optimize the instantaneous torque performance of an SRM. The algorithm aims to reduce the torque ripple and dynamic torque response of the motor when using a proportional-integral controller. In [10], a modified hybrid whale optimization algorithm is used to reduce the torque ripple for a wide speed range. The optimization considers the limitation of the controller and phase current commutation and improves the desired dynamic performance by optimizing conduction angles. In [11], an offline optimization is developed to maximize average torque by finding the minimum of single-variable function on a fixed interval. The optimization was done for a wide current reference and speed range. In [12], a multiobjective optimization is used to control the turn-OFF angle using the torque ripple and copper loss objectives. The proposed optimization does not require the motor parameters and the turn-ON angle is selected based on the turn-OFF angle. In paper [13], multiobjective optimization is used to improve three objectives using an individual weighted method for motoring mode: average torque, torque ripple, and copper loss. The conduction angles are optimized to be used by a conduction angle regulating scheme and a hysteresis controller. In paper [14], the conduction angles are selected using a teaching and learning based optimization technique and Grey Wolf optimization to maximize the average torque and minimize torque ripple. In paper [15], conduction angles are selected by maximizing the torque per ampere objective to improve the motor efficiency. The optimization is accomplished using a direct instantaneous torque control which allows for simple implementation. In [16], an elitist-mutated multiobjective particle swarm optimization is used to select the conduction angles to minimize torque ripple while maximizing the average torque. In [17], an artificial intelligence-based control is used to minimize the torque ripple by selecting conduction angles based on the operating speed. The optimization specifically uses the turn-OFF angle to change the behavior of the demagnetizing current.

For generating mode, no specific control scheme has been developed to improve the amount of power returned to the source for a specific amount of torque extracted while improving efficiency. However, there is literature using current control to select conduction angles for wind generation applications, but do not modify the control scheme for soft-switching and multiple objectives at the same time. In [18], an SRM is used with max power point tracking, but the current control was accomplished using hard-switching and does not take advantage of free-wheeling current in generating mode. In [19] and [20], conduction angles are selected for generation applications for maximum efficiency, but only uses single pulse control which can be only utilized effectively above the base speed. In [21], an SRM is used for traction applications with conduction angles being selected for generating mode via a weighted multiobjective optimization, but the same motoring mode control is used in generating mode and the objectives selected are not specific for generating mode.

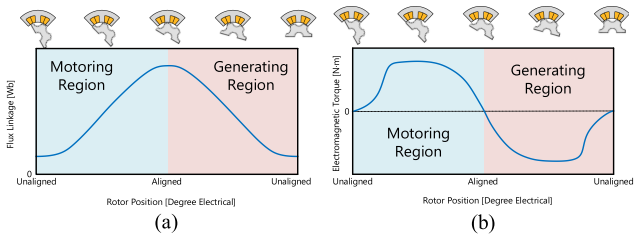

FIGURE 1. Static characteristic at different rotor positions. (a) Flux linkage. (b) Electromagnetic torque.

As any electric motor, the SRM is capable of four-quadrant operation and the work done to improve the motoring performance does not directly translate to generating mode. Generating mode requirements can be different from the motoring mode and little work has been done in the literature with regards to this subject. This article presents optimization objectives to specifically improve the generating mode of operation by maximizing the amount source current returned to the source while minimizing the torque. In Section 2, motoring and generating mode are compared for different conduction cases using the phase current, induced voltage, and torque behavior. Section III introduces generating specific optimization objectives which are developed using an exhaustive conduction angle search for a specific rotor speed and current reference. The generating mode specific objectives are compared to motoring mode. In Section IV, the experimental results are presented to validate the generating mode specific optimization objectives. The generating mode specific optimization objectives are also experimentally compared to motoring objectives. Finally, Section V concludes the article.

II. COMPARING MOTORING AND GENERATING MODE CONTROL

Similar to conventional electric motors, an SRM can operate in generating mode. In motoring mode, a phase of an SRM is excited with current when the phase flux linkage increases with rotor position, as shown in Fig. 1. When the rotor is aligned due to phase excitation, an external force is required to move the rotor beyond alignment, as any position before and past alignment will result in larger magnetic reluctance. For generating mode operation, an external force should oppose the forces exerted on the rotor pole from the magnetic field. Then, a negative torque is applied to that prime mover drawing power from it. The energy transfers from the prime mover to the magnetic circuit. It is converted into electrical energy and fed back to the power source by regulating the phase current with an asymmetric bridge converter [22], [23]. In generating mode, a phase of an SRM is excited when the phase flux linkage decreases with rotor position, as shown in Fig. 1.

The performance of a 4-phase 8/6 SRM is compared for motoring and generating mode of operations using conduction angle control. In Table 1, the properties of the 4-phase 8/6 SRM are provided. The conduction angles are selected for motoring mode, then are either shifted by 180^o electrical

TABLE 1. 4-phase 8/6 SRM properties.

Parameter	Value
Number of phases	4
Number of stator and rotor poles	8/6
Stack height	90 mm
Base speed	6000 r/min
Phase resistance	0.076 Ω
Rated DC-link voltage	300 V
Rated power	5.2 kW

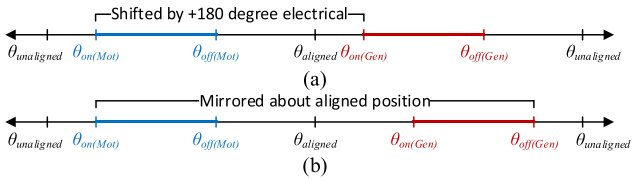

FIGURE 2. Comparing motoring and mode using (a) conduction angles shifted by 180° and (b) conduction angles mirrored around the aligned position at 180°.

TABLE 2. Current control simulation parameters.

Parameter	Value	
Speed	4000 r/min	
Current reference	20 A	
Motoring early conduction	$\theta_{on} = 10^o$	$\theta_{off} = 120^o$
Motoring late conduction	$\theta_{on} = 60^o$	$\theta_{off} = 170^o$
Generating early conduction	$\theta_{on} = 190^o$	$\theta_{off} = 300^o$
Generating late conduction	$\theta_{on} = 240^o$	$\theta_{off} = 350^o$

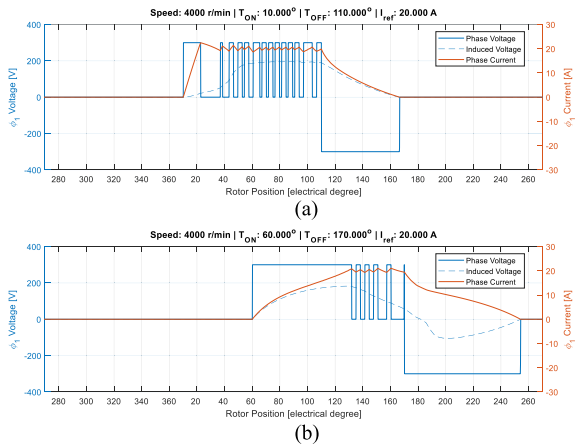

FIGURE 3. Phase current waveform for motoring mode. (a) Early conduction angles defined in Table 2. (b) Late conduction angles defined in Table 2.

or mirrored along the aligned position to obtain generating mode conduction angles. This is done to show how motoring and generating modes compare for the same conduction period using conduction angle control. A sample of the shifted and mirrored conduction angles are shown in Fig. 2. The motoring and generating performances are compared using soft-switching at 4000 r/min using the conduction angles presented in Table 2.

In Fig. 3(a), the phase current is shown for motoring mode with early conduction angles of 10° and 110° electrical. The turn-ON angle occurs closer to the unaligned position which

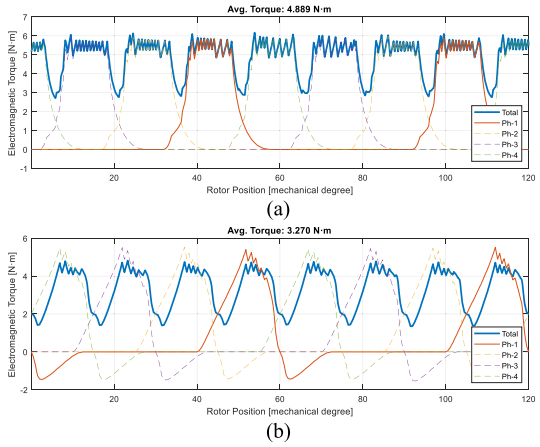

FIGURE 4. Torque waveform for motoring mode. (a) Early conduction angles defined in Table 2. (b) Late conduction angles defined in Table 2.

results in a much faster rate of change of current aided by the low phase inductance. However, at the turn-OFF, the inductance is higher due to the aligned position, resulting in the phase current to demagnetize much slower. In Fig. 3(b), late motoring conduction angles of 60° and 170° electrical are used. With delayed motoring conduction, the turn-ON angle occurs much later than the unaligned position, which results in the phase current to rise slower. Additionally, the turn-OFF angle is also close to the aligned position, which results in a much slower rate of change in phase current.

In Fig. 4(a) and (b), the phase and total torque are plotted for early and late motoring conduction. As the phase current in the early motoring case was able to rise and quickly decay, the significant torque ripple contribution was due to the commutation region. In the late conduction case, torque ripple is higher. This is due to the phase current demagnetizing within the generating region which occurs past the aligned position and that results in negative torque production. In motoring mode, the torque ripple can be reduced, and average torque can be improved by specifically selecting conduction angles based on the operating speed.

Equation (1) shows the soft switching control conditions applied in motoring mode, where $V_{\text{ph}}(k)$ is the phase voltage at the given time instant, $V_{\text{ph}}(k-1)$ is the phase voltage at the previous time instant, V_{DC} is the dc-link voltage, i_{ph} is the phase current, and I_{upper} and I_{lower} are the upper and lower current hysteresis bands, respectively. To regulate the current within the hysteresis band, freewheeling mode of the asymmetric bridge converter is used where only one switch is turned OFF. In motoring mode, this reduces the phase current. In Fig. 5, the same soft-switching control in (1) is applied for early generation using conduction angles of 190° and 300° electrical at 4000 r/min. After the turn-ON angle is applied, the phase current begins to rise. When the phase current reaches the upper hysteresis band, the asymmetric bridge converter short circuits the phase in freewheeling mode. However, in generating mode, the phase current rises with a larger slope rather than decreasing as it would in motoring mode. This

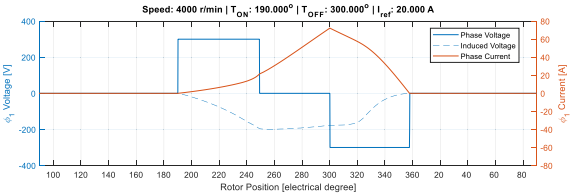

FIGURE 5. Phase current waveform for early generation mode conduction when soft switching for motoring mode is applied to generating mode.

is because, in generating mode, when zero phase voltage is applied, the induced voltage is negative. As the induced voltage is smaller than phase voltage, using (2), the resulting rate-of-change of phase current is positive. Thus, the phase current increases. At the turn-OFF angle, negative dc-link voltage is applied to the phase. As the magnitude of the induced voltage is smaller than the magnitude of the phase voltage, the phase current reduces. This shows that the soft-switching in motoring mode cannot be applied in generating mode; otherwise it results in uncontrolled peak current. For soft-switching to work in generating mode, some modifications need to be applied for current regulation

$$V_{\text{ph}}(k) = \begin{cases} 0 & \text{excitation signal} \le 0 \cap i_{\text{ph}} \le 0 \\ -V_{\text{DC}} & \text{excitation signal} \le 0 \cap i_{\text{ph}} > 0 \\ 0 & \text{excitation signal} > 0 \cap i_{\text{ph}} \ge I_{\text{upper}} \\ +V_{\text{DC}} & \text{excitation signal} > 0 \cap i_{\text{ph}} < I_{\text{lower}} \\ V_{\text{ph}}(k-1) & \text{excitation signal} > 0 \cap I_{\text{upper}} > i_{\text{ph}} \ge I_{\text{lower}} \\ 0 & \text{else} \end{cases} \tag{1}$$

$$\frac{V-\varepsilon}{L} = \frac{di}{dt}, \varepsilon = i\frac{\partial L(\theta)}{\partial \theta}\omega_r \tag{2}$$

$$V_{\text{ph}}(k) = \begin{cases} 0 & \text{excitation signal} \le 0 \cap i_{\text{ph}} \le 0 \\ -V_{\text{DC}} & \text{excitation signal} \le 0 \cap i_{\text{ph}} > 0 \\ -V_{\text{DC}} & \text{excitation signal} > 0 \cap i_{\text{ph}} \ge I_{\text{upper}} \\ 0 & \text{excitation signal} > 0 \cap i_{\text{ph}} < I_{\text{lower}} \\ V_{\text{DC}}^{*} & \text{excitation signal} > 0 \cap i_{\text{ph}} < I_{\text{lower}}* \\ V_{\text{ph}}(k-1) & \text{excitation signal} > 0 \cap I_{\text{upper}} > i_{\text{ph}} \ge I_{\text{lower}} \\ 0 & \text{otherwise.} \end{cases}$$

$$* \text{ Used for initial excitation.} \tag{3}$$

Equation (3) shows the modified hysteresis controller to control the phase current with soft-switching in generating mode. The main difference is that when the phase current is higher than the upper hysteresis band, negative dc-link voltage is applied rather than zero. When a negative dc-link voltage is applied, as the induced voltage magnitude is lower than the phase voltage magnitude especially at lower speed operation, the phase current reduces. As the phase voltage is negative, the phase current is supplied to the source. However, at higher speeds the magnitude of the induced voltage can be greater

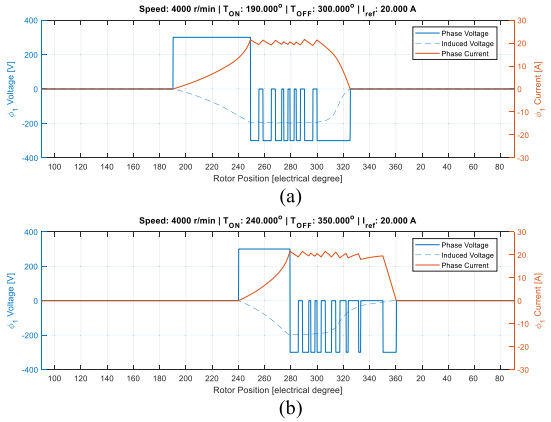

FIGURE 6. Phase current waveform using current control using proposed generating specific switching for (a) early conduction angles defined in Table 2 and (b) late conduction angles defined in Table 2.

than the dc-link voltage, resulting in the phase current to increase, depending on the rotor position and phase current magnitude.

Hence, there is a fundamental difference in current control for motoring and generating mode of operations of an SRM. In motoring mode, when the phase current is smaller than the lower hysteresis band, positive dc-link voltage is applied to increase the phase current. In generating mode operation in (3), freewheeling mode is applied where the phase winding is short-circuited. This results in the magnitude of the induced voltage being larger than the phase voltage. The phase current rises. However, since the phase winding is not connected to the source, no power supplied or drawn from the electrical source. The rise of the phase current is due to the power drawn from the prime mover. With hysteresis control model in (3), the only time current is drawn from the power source is during the initial phase excitation where positive dc-link voltage is applied across the phase winding. This is essential, as an SRM does not have an independent source of excitation and it needs to draw the initial excitation from the source.

In Fig. 6(a), the hysteresis control conditions in (3) are used for early generation conduction angles of 190° and 300° electrical. In generating mode, the turn-ON angle occurs closer to the aligned position, which results in a small rate of change in phase current. While the turn-OFF occurs much closer to the unaligned position which results in a rapid decay in the phase current. In Fig. 6(b), the soft-switching hysteresis conditions in (3) are used to control the phase current in generating mode with later conduction angles of 240° and 350° electrical. In Fig. 7(a) and (b), the torque waveforms are plotted for generating mode with early and late conductions. When the current and torque waveforms for motoring and generating modes are compared, it can be observed that the waveforms are not the same. This means that if the conduction angles calculated for the motoring mode are shifted or mirrored to generating mode, they might not provide the same output. Instead, conduction angles should be calculated specifically for generating mode of operation.

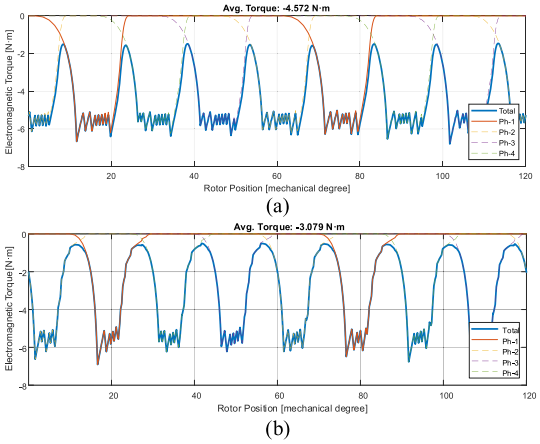

FIGURE 7. Torque waveform using current control using proposed generating specific switching for (a) early conduction angles defined in Table 2 and (b) late conduction angles defined in Table 2.

III. OPTIMIZING OBJECTIVES TO IMPROVE GENERATING MODE PERFORMANCE

The classical control in a switched reluctance machine requires the selection of conduction angles for a given operating condition. The selection of the conduction angles for the control of an SRM can be accomplished by maximizing or minimizing specific fitness functions using an optimization algorithm. For SRMs, the average torque, RMS value of torque ripple, and RMS value of phase current can be the objectives used for the motoring mode region. The average torque can be determined using the following:

$$T_{\text{avg}} = \frac{1}{\theta_2 - \theta_1} \int_{\theta_1}^{\theta_2} T(\theta)\, d\theta \tag{4}$$

where T_{avg} is the average torque, $T(\theta)$ is the instantaneous rotor torque at a specific rotor position, and θ_1 and θ_2 are rotor positions representing the start and end of an electrical cycle. The RMS value of torque ripple (ΔT_{RMS}) and RMS value of phase current (I_{RMS}) are defined in in the following equations:

$$\Delta T_{\text{RMS}} = \sqrt{\frac{1}{\theta_2 - \theta_1} \int_{\theta_1}^{\theta_2} \left(T(\theta) - T_{\text{avg}}\right)^2 d\theta} \tag{5}$$

$$I_{\text{RMS}} = \sqrt{\frac{1}{\theta_2 - \theta_1} \int_{\theta_1}^{\theta_2} I^2(\theta)\, d\theta} \tag{6}$$

where $I(\theta)$ is the instantaneous phase current for a given rotor position. These optimization objectives can also be configured as a relation of one another to be used in a single fitness function. For example, the average torque ripple and RMS value of phase current can be configured as $T_{\text{avg}}/\, I_{\text{RMS}}$ to optimize for maximum torque per ampere representing the motor efficiency. The optimizer can also be provided with linear and nonlinear constraints to limit the range of conduction interval and to limit the phase current below its maximum value.

A. OPTIMIZATION TO MAXIMIZE ABSOLUTE AVERAGE TORQUE AND MINIMIZE TORQUE RIPPLE

In an SRM drive, typical objectives that are used to determine the conduction angles in motoring mode of operation are maximizing the average torque and minimizing the RMS value of torque ripple. These objectives are targeted in motoring mode to achieve a high torque output and smoother operation with lower torque ripple. In this section, these objectives are applied to generating mode of operation, to observe how they impact the performance. The optimizer is supplied with various speed and current reference cases to determine different working conditions and develop a torque-speed map.

For the generating mode cases, the torque ripple is minimized. Since the torque should be negative in generating mode, the average torque is minimized unlike the motoring mode of operation. The constraints for the optimization are shown in (7). The turn-ON conduction angle is constrained between 90° and 270° electrical, and the turn-OFF conduction angle is constrained between 270° and 360° electrical. The conduction interval is limited between 90° and 180°. The current constraint is 60 A_{RMS} to mitigate wire insulation limit

$$\begin{aligned} 90^{\text{o}} \le \theta_{\text{on}} \le 270^{\text{o}} \qquad & 90^{\text{o}} \le \theta_{\text{off}} - \theta_{\text{on}} \le 180^{\text{o}} \\ 270^{\text{o}} \le \theta_{\text{off}} \le 360^{\text{o}} \qquad & I_{\text{RMS}} \le 60 \text{ A}. \end{aligned} \tag{7}$$

In Fig. 8, the torque-speed maps are shown for generating mode current control with the absolute average torque maximized and torque ripple minimized. The percent torque ripple reduces as the average torque increases, shown in Fig. 8(a). With the average torque increasing, the RMS value of torque ripple increases as shown in Fig. 8(b). As the rotor speed increases, the turn-ON angles advance before the aligned position, as shown in Fig. 8(c) and turn-OFF angle moves away from the unaligned position, as shown in Fig. 8(d). With the average torque maximized and torque ripple minimized, the conduction interval is maximized for the entire torque-speed region as shown in Fig. 8(f). In generating mode, after the base speed of 6000 r/min the torque does not decrease. This is due to generating mode resulting in a negative induced voltage. At higher speeds the induced voltage is more negative than the dc-link voltage resulting in the phase current to continue to rise as shown in Fig. 9.

Maximizing the absolute value of average torque and minimizing the torque ripple using multiobjective optimization to select the conduction angles does not specifically improve the generating mode performance as the objectives are more specific to the motoring mode operation. However, motoring mode objectives does not provide information on the current supplied to the source, which is an important performance parameter in generating mode. Therefore, the optimization objectives need to be updated to specifically improve the generating mode performance.

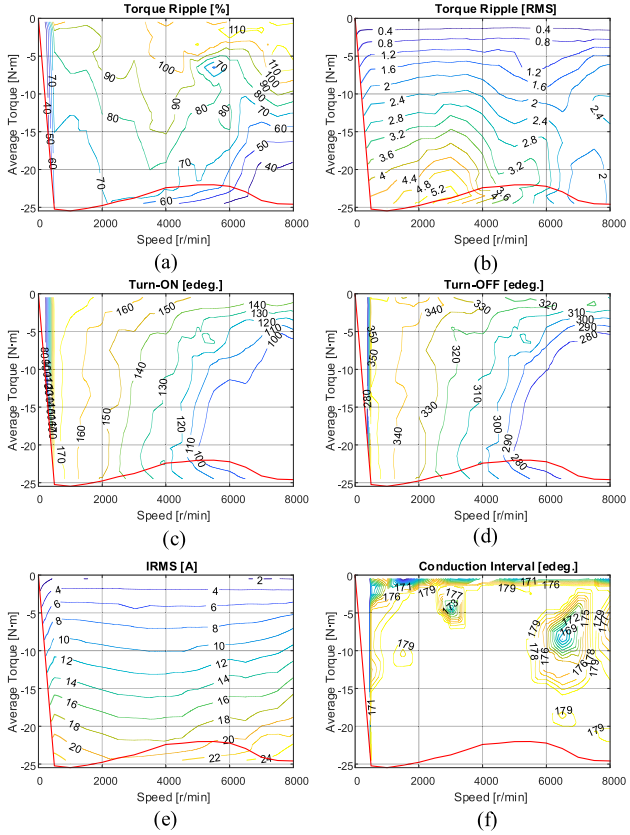

FIGURE 8. Torque-speed map of an 8/6 SRM in generating mode with the absolute average torque maximized and torque ripple minimized. (a) Percent torque ripple contour. (b) Torque ripple RMS contour. (c) Turn-ON angle contour. (d) Turn-OFF angle contour. (e) Phase current RMS contour. (f) Conduction interval contour.

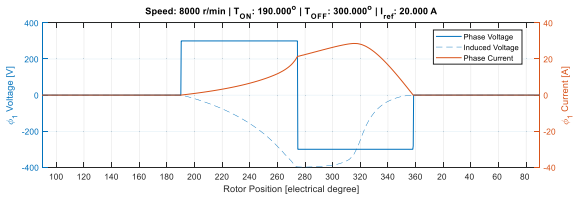

FIGURE 9. Phase current using current control at high-speed in generation mode.

B. SELECTING OPTIMIZATION OBJECTIVES SPECIFIC TO GENERATING MODE OPERATION

To determine optimization objectives to improve generating mode performance, an exhaustive search is carried out first. The exhaustive search for conduction angles is conducted for a given current reference and rotor speed. Then, all potential turn-ON and turn-OFF conduction angles are investigated to map out the specific objectives to be explored. For the exhaustive search, an additional model constraint needs to be considered for generating mode. In the optimization constraints for generating mode in (7), the turn-OFF angle is limited from 270° to 360° electrical. For exhaustive search, it should be investigated whether the case when the turn-OFF angle extending beyond unaligned position would improve the

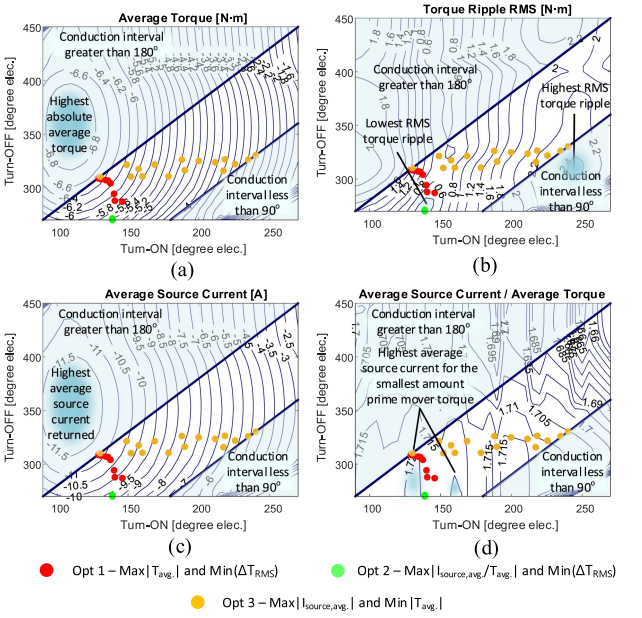

FIGURE 10. Exhaustive simulation result at 5000 r/min and 20 A reference in generating mode with: (a) average torque, (b) torque ripple RMS, (c) average source current, and (d) average source current per torque.

performance especially at high-speed operation. Therefore, the constraints are revised as in (8), and the minimum and maximum conduction interval constraints are removed

$$90^{\circ} \leq \theta_{\text{on}} \leq 270^{\circ}$$
$$270^{\circ} \leq \theta_{\text{off}} \leq 450^{\circ}. \tag{8}$$

The exhaustive search is done for soft-switching current control for generating mode at 5000 r/min with a current reference of 20 A. The exhaustive simulation contours plots in Fig. 10 show the conduction angles along with shaded regions indicating turn-ON and turn-OFF angle combinations that exceed the constraints in (7). Fig. 10(a) shows the average torque contour as a function of turn-ON and turn-OFF angles. The highest absolute average torque is when the turn-ON angle is between 90° and 125° electrical and turn-OFF angle is near the unaligned position (360° electrical). Also, the highest absolute average torque is in the region where the conduction interval is larger than 180° electrical. Fig. 10(b) shows the torque ripple RMS contour. The highest torque ripple occurs around when the turn-ON angle is 245° electrical and the turn-OFF angle is around 315° electrical. The highest RMS torque ripple occurs in a region where the conduction period is less than 90° electrical. An additional measurement contour is plotted in Fig. 10(d) by combining the average source current divided by the average torque. This was done to minimize the total number of optimization objectives from three to two. By using the average source current divided by the average torque as the first objective and RMS value of torque ripple as the second objective, the optimizer can consider all three objectives but not independently. The proposed generating specific optimization objective can be expressed as follows:

$$\text{Obj}_4 = \frac{I_{\text{source,avg}}}{T_{\text{avg}}} \tag{9}$$

where $I_{\text{source,avg}}$ is the average source current, and T_{avg} is the average torque. From Fig. 10(d), it can be seen that Obj_4 is maximum at the early turn-ON and turn-OFF angles and does not occur at the points where the absolute average torque and source currents are maximum. The region where the maximum absolute average torque and source current occur is where the conduction interval is larger than 180° electrical as shown in Fig. 10(a) and (c). However, in Fig. 10(d), the maximum value of Obj_4 appears in a region where the conduction interval is within the constraints presented in (7). In addition, the minimum RMS value of torque ripple occurs relatively close to where Obj_4 is maximum. This implies that, if a multiobjective optimization is to be used involving Obj_4 and torque ripple, a much smaller Pareto front can be created.

In Fig. 10, there are scatter points on all exhaustive search contour plots to show the trends for different optimization objectives. The red points (Opt 1) represent conduction angles when the multiobjective optimization is carried out for the objectives: 1) maximizing the absolute average torque and 2) minimizing the torque ripple. These objectives are similar to the motoring mode of operation. For the red points, the conduction constraints in (7) are utilized which enable delaying the turn-OFF angle beyond unaligned position. When observing the optimization results in Fig. 10(a) and (b) shown with the red points, the turn-ON and turn-OFF angles are distributed between the two regions where the absolute average torque is maximized and torque ripple is minimized, confirming the optimizer is functioning correctly.

In Fig. 10, the green points (Opt 2) represent the proposed generating specific optimization objectives of 1) maximizing the average source current per absolute average torque and 2) minimizing the torque ripple. With these objectives, the results are far more concentrated to one set of conduction angles. When observing the green points in Fig. 10(b) and (d), the torque ripple is minimized while the average source current per average torque is maximized. The new optimization objectives in Opt 2 essentially extract and return the most amount of source current for the smallest absolute average torque and minimize the torque ripple while doing so.

In Fig. 10, the orange points (Opt 3) represent conduction angle points which are obtained using the following optimization objectives: 1) minimizing the absolute average torque and 2) maximizing the source current. These objectives tend to maximize the source current per average torque but in two independent objectives in a multiobjective optimization. However, the orange points in Opt 3 create a Pareto front between the conduction period limitation represented in (7) for the two objectives. Furthermore, the Pareto front is broad due to the solutions being on the polar ends of the conduction angle range making it far more difficult to choose working conduction angles. The large Pareto front is created between the two objectives consisting of 20 working conduction angle conditions and the GA optimizer's initial population size was also 20. This means that each initial point converged to a unique solution between the two objectives. However, the optimization ignores the RMS value of torque ripple consideration, which results in all the working conditions being selected between the two objectives to have significant torque ripple compared to the optimization results found earlier.

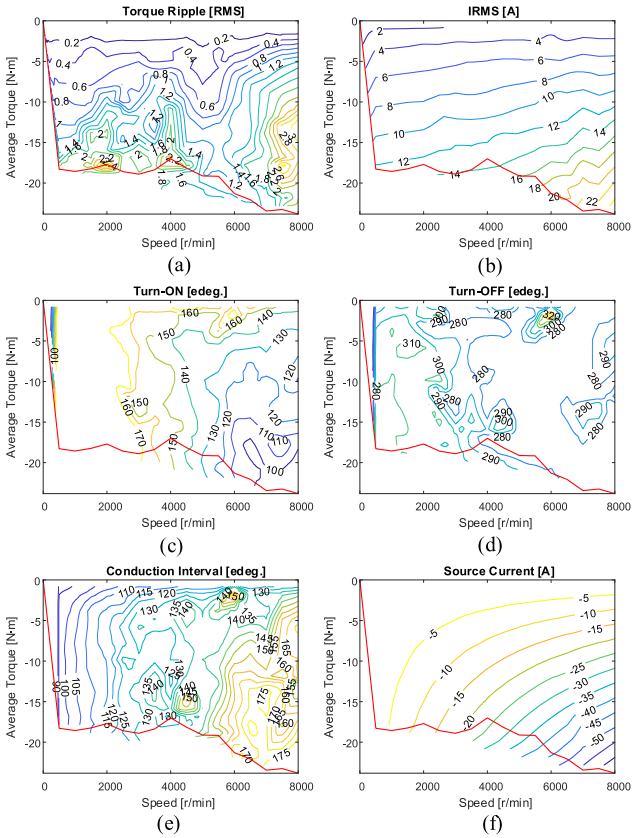

FIGURE 11. Torque-speed map of an 8/6 SRM in generating mode with the average source current per torque maximized and torque ripple minimized. (a) Torque ripple RMS contour. (b) Phase current RMS contour. (c) Turn-ON angle contour. (d) Turn-OFF angle contour. (e) Conduction interval contour. (f) Average source current contour.

Notably, the source current, absolute average torque, and torque ripple all need to be considered in generating mode. As it would be a lot more challenging to find a solution from a Pareto front with three separate objectives, the most effective optimization results were obtained by maximizing the source current per absolute torque and minimizing the torque ripple.

C. PROPOSED OPTIMIZATION TO MAXIMIZE SOURCE CURRENT PER TORQUE AND MINIMIZE TORQUE RIPPLE

The multiobjective optimizer is used to generate conduction angles for the new objectives specific to generating mode. The results are shown in Fig. 11.

In Fig. 11(b), the phase current contours are shown, and the RMS phase current reduced from 14 to 12 A using the proposed optimization objectives (Opt 2) compared to the old optimization objectives (Opt 1) using soft switching in

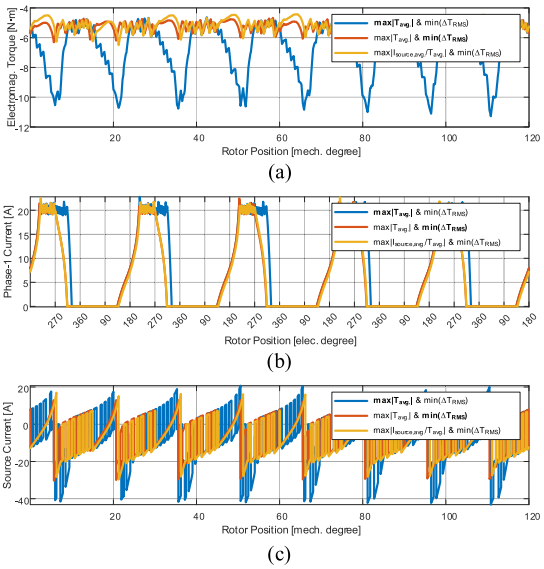

FIGURE 12. Generating mode results at 20 A and 4000 r/min. (a) Electromagnetic torque. (b) Phase current. (c) Source current.

Fig. 8(e); for the same torque-speed point of 5000 r/min and –14 N·m. In Fig. 11(c) and (d), the turn-ON and turn-OFF contours are plotted using the new optimization objectives. Opt 2 optimization objectives do not advance turn-ON and OFF conduction angles significantly until higher operating speeds. With Opt 1 objectives the conduction angles were advanced even at lower speeds. This is because the maximum source current per torque and minimum torque ripple points occurs around 130° and 290° electrical for the turn-ON and turn-OFF conduction angles, as shown in Fig. 8(c) and (d). The proposed optimization objectives (Opt 2) stay within that conduction region while the SRM operates in the constant torque region. This maximizes the fitness function associated with the two objectives. At higher speeds, the phase current behavior is the same as single pulse mode due to relationship between the dc-link voltage and induced voltage. This results in the optimizer to advance the conduction angles to achieve the proposed generating specific objectives, because an earlier turn-ON angle contributes to a higher current magnitude.

As shown in Fig. 11(e), the conduction interval expands as the rotor speed increases to maintain torque ripple performance. The reduction in conduction interval results in a lower phase RMS current with Opt 2 objectives as compared to Opt 1 objectives, for majority of the torque-speed envelope.

IV. COMPARISON OF GENERATING MODE PERFORMANCE WITH THE PROPOSED OPTIMIZATION

In Fig. 12, Opt 1 objectives for $\max|T_{\text{avg}}|$ and $\min(\Delta T_{\text{RMS}})$ are compared to the proposed Opt 2 objectives of $\max|I_{\text{source,avg}}/T_{\text{avg}}|$ and $\min(\Delta T_{\text{RMS}})$ for the soft-switching current control, using the torque, phase current, and source current waveforms. Two different results for Opt 1 are shown. The blue waveforms are for the results on the Pareto front

TABLE 3. Comparison of optimization results at 20 A and 4000 r/min in generating mode.

Optimization objectives	Opt 1: $\max\|T_{avg}\|$ and $\min(\Delta T_{RMS})$	Opt 1: $\max\|T_{avg}\|$ and $\min(\Delta T_{RMS})$	Opt 2: $\max\|I_{source,avg}/T_{avg}\|$ and $\min(\Delta T_{RMS})$
RMS phase current [A]	7.815	6.365	6.215
Avg. torque [N·m]	-6.782	-5.198	-5.129
Torque ripple RMS [N·m]	1.781	0.275	0.380
Avg. source current [A]	-9.297	-7.123	-7.038
Source current per torque [A/N·m]	1.371	1.370	1.372
Avg. mech. power [kW]	2.84	2.18	2.15
Avg. elec. power [kW]	2.786	2.144	2.113

TABLE 4. Comparison of optimization results at 20 A and 8000 r/min in generating mode.

Optimization objectives	Opt 1: $\max\|T_{avg}\|$ and $\min(\Delta T_{RMS})$	Opt 2: $\max\|I_{source,avg}/T_{avg}\|$ and $\min(\Delta T_{RMS})$
RMS phase current [A]	14.730	11.808
Avg. torque [N·m]	-11.833	-10.252
Torque ripp. RMS [N·m]	2.518	2.356
Avg. source current [A]	-32.637	-28.290
Source current per torque [A/N·m]	2.758	2.759
Avg. mech. power [kW]	9.91	8.59
Avg. elec. power [kW]	9.899	8.598

where average torque is given priority. The red waveforms are from the same Pareto front, but torque ripple is given priority.

As shown in Fig. 12(a), the proposed optimization objectives result in lower torque ripple. Additionally, the optimization results in a solution that does not have large variation in conduction angles. In Fig. 12(b), the phase current performance is shown. The proposed optimization (Opt 2) reduces the conduction interval which reduces the RMS phase current. In Fig. 12(c), the source current is plotted to compare the multi-objective optimizations. The source current from the proposed optimization (Opt 2) is equivalent to Opt 1 which prioritized torque ripple minimization.

Table 3 shows the performance results for Opt 1 and Opt 2 objectives at 20 A current reference and 4000 r/min rotor speed. The proposed multiobjective optimization results in the highest average source current per average torque. The proposed optimization Opt 2 results in a 1.38% reduction in the mechanical power drawn when compared to Opt 1. Opt 2 results in marginally less electrical power supplied but reduces the RMS phase current by 2.36%. Additionally, Opt 2 also converges to a smaller set of working conduction angles that specifically improve the SRM generating mode performance.

In Fig. 13, the same comparison is applied for high-speed operation at 8000 r/min. In Fig. 13(a), the highest absolute average torque is observed for Opt 1. As shown in Fig. 13(b), the phase current for Opt 2 has smaller magnitude as compared to Opt 1 objectives.

Table 4 shows the performance results for the two cases. The proposed optimization objectives of $\max|I_{\text{source,avg}}/T_{\text{avg}}|$

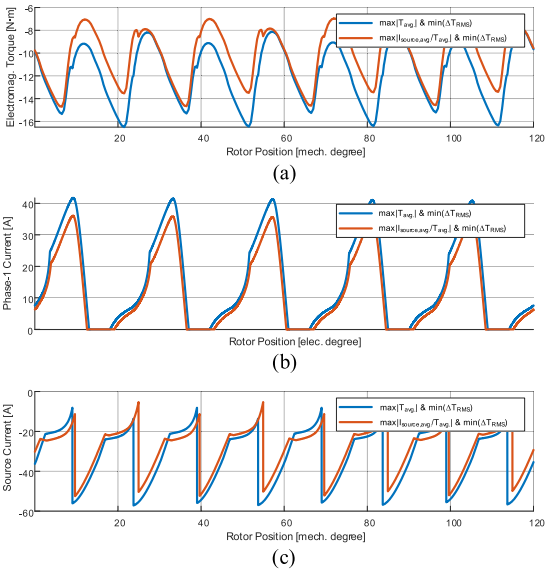

FIGURE 13. Generating mode results at 20 A and 8000 r/min. (a) Electromagnetic torque. (b) Phase current. (c) Source current.

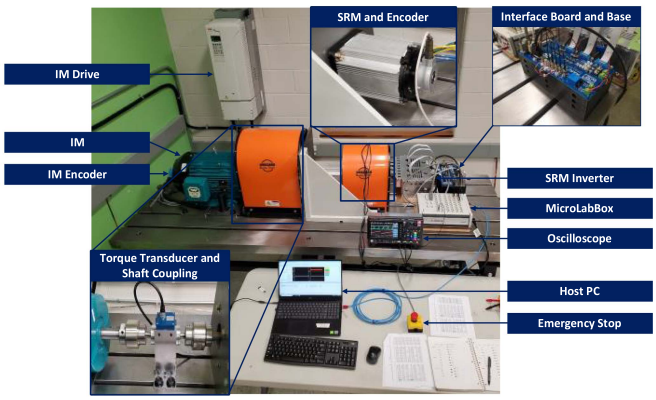

FIGURE 14. Experimental SRM setup to validate the proposed generating mode objectives.

and $\min(\Delta T_{\text{RMS}})$ improve the generating mode performance by reducing the amount of prime mover torque extracted and minimizing the torque ripple when compared to the $\max|T_{\text{avg}}|$ and $\min(\Delta T_{\text{RMS}})$ objectives. The proposed optimization (Opt 2) also has a slightly higher average source current per average torque despite returning marginally less source current when compared to Opt 1. Using Opt 2, the mechanical power drawn is reduced but relatively less when compared to the electrical power supplied back. Additionally, the proposed optimization objectives reduce the RMS phase current by 19.83% when compared to Opt 1, while generating a smaller Pareto front.

TABLE 5. Experiment SRM parameters.

Parameter	Value
Configuration	12/8
Rated Speed	2200 r/min
Voltage	72 V
Torque	21.7 N·m

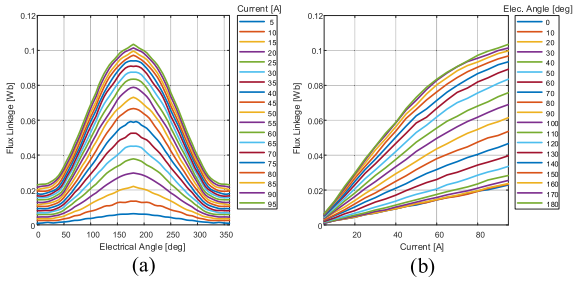

FIGURE 15. Experimental flux linkage characteristics of the 12/8 SRM as a function of (a) electrical rotor position and (b) phase current.

V. EXPERIMENTAL VALIDATION

An experimental setup is developed as shown in Fig. 14 to perform experimental validation of the generating mode optimization scheme. The setup consists of an SRM and IM coupled through a torque transducer using flexible shaft coupling. The control and power conversion of the IM is provided by a dedicated industrial motor drive and an H-bridge converter for the SRMs excitation. The control of the SRM is provided by a dSpace MicroLabBox rapid prototyping controller. The rotor position and speed of the SRM is captured by an absolute encoder, and the IM speed is measured using an incremental encoder. All the sensor feedback is provided to the rapid prototype controller to be processed. Table 5 shows the key parameters of the 3-phase SRM that is used for experimental validation.

A. EXPERIMENTAL CHARACTERIZATION OF STATIC FLUX LINKAGE AND TORQUE PROFILES

The 3-phase 12/8 SRM used to perform the experimental results has an unknown internal geometry. With this limitation, the motor geometry cannot be implemented in FEA to obtain the static characteristics which are needed for the dynamic modeling of the motor. Therefore, the static characteristics of the motor are determined through indexing utilizing the voltage pulse method at different rotor position for one electrical cycle [24]. The flux-linkage is then determined using the phase voltage, current, and resistance relation

$$\lambda(\theta, i) = \int_0^t [V(t) - Ri(t)]\, dt \tag{10}$$

where the flux linkage λ can be calculated for a fixed rotor position θ and current reference i by solving the time integral. Using a micro-ohmmeter, the phase resistance, R is measured as 23.175 mΩ. Fig. 15 shows the experimental flux linkage measurement results.

The static torque is then calculated using the flux linkage characteristics. Using (11), first co-energy is calculated from

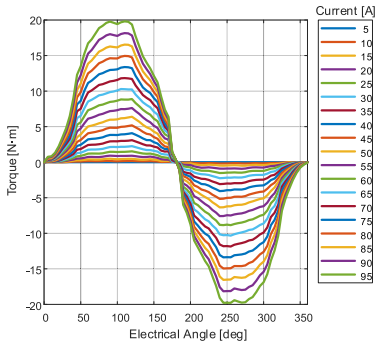

FIGURE 16. Experiment static torque characteristics of 12/8 SRM.

TABLE 6. Comparison torque and measured torque comparison for different rotor positions with a locked rotor.

Current [A]	Calculated torque [N·m]	Measured torque [N·m]	Absolute error [%]
20	0.923	1.000	8.292
30	2.138	2.300	7.553
40	3.840	4.100	6.762
50	5.980	6.500	8.702
60	8.480	9.250	9.074
70	11.364	12.300	8.240
80	14.626	15.800	8.030
90	18.010	19.300	7.162

flux linkage and then the electromagnetic torque is calculated from co-energy

$$W_c = \int \lambda di \quad T_e = \left.\frac{\partial W_c}{\partial \theta}\right|_{i=\text{const.}} \tag{11}$$

Fig. 16 shows the static electromagnetic torque calculated from flux linkage for the 12/8 SRM for one complete electrical cycle. A quick validation of the static torque characterization was conducted by measuring the torque using the torque transducer and comparing it to the torque calculated from the flux-linkage. In Table 6, the percent error is shown between the measured and calculated torque at different rotor positions. The absolute error is below 10% for all cases.

For the validation of the measured motor characteristics, the transient behavior of the experimental and simulation data needs to be compared with dynamic results. In Fig. 17, the simulation and experimental results are compared for 600 r/min and 40 A current reference, for the turn-ON and OFF conduction angles of 143.47° and 323.46° electrical, respectively. In Fig. 17(a), the experimental and simulation phase currents match closely. There is a slight difference at the initial excitation because the line regulation of the bidirectional power supply results in fluctuations in the dc-link voltage. As shown in Fig. 17(b), the source current behavior matches closely. The difference can be attributed to the bidirectional power supply filtering the source current with a single pole low-pass filter (cut-off frequency of 2.1 kHz). In Fig. 17(c), the experimental torque does not show the ripples observed as the limited bandwidth of the torque transducer filters the high frequency torque ripple, but the average torque matches closely.

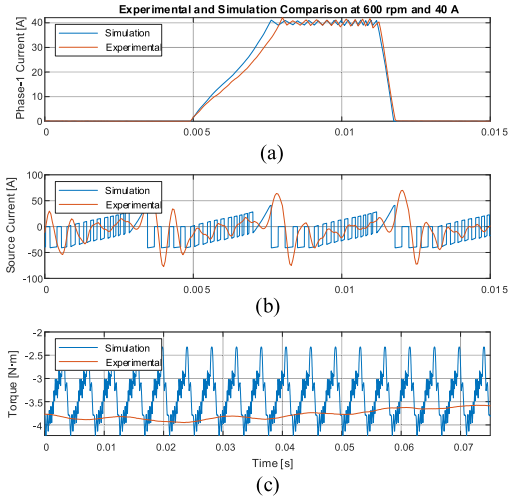

FIGURE 17. Experimental and simulation results at 600 r/min and 40 A current reference. (a) Phase current. (b) Source current. (c) Shaft torque.

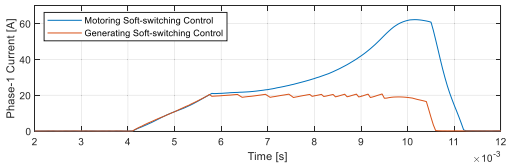

FIGURE 18. Generating mode phase current using the motoring and generating specific soft-switching control.

Another experiment is applied to validate the soft switching method proposed in (3) for generating mode. As shown in Fig. 18, if motoring mode soft switching in (1) is applied in generating, the peak current cannot be controlled. When the generating mode soft switching in (3) is applied, peak phase current can be regulated.

B. EXPERIMENTAL VALIDATION OF OPTIMIZATION OBJECTIVES WITH 20 V SUPPLY VOLTAGE AT 600 R/MIN

In Fig. 19, the experimental results for the optimization objectives in Opt 1 of $\max|T_{\text{avg}}|$ and $\min(\Delta T_{\text{RMS}})$ are compared to the proposed generating specific optimization objectives in Opt 2 of $\max|I_{\text{source,avg}}/T_{\text{avg}}|$ and $\min(\Delta T_{\text{RMS}})$. In Fig. 19(a), the conduction period for Opt 2 is smaller than Opt 1. Specifically, the turn-OFF occurs earlier in the proposed optimization objectives. In Fig. 19(c), the proposed generating specific objectives in Opt 2 extract much lower prime mover torque for a similar amount of source current when compared to the objectives in Opt 1. In Table 7, the performance of Opt 1 and proposed optimization Opt 2 objectives are compared. With Opt 2, the phase current is reduced by 14.7% which would result in smaller copper loss. Since the speed and phase current is low in this case, the average source current is slightly above zero for both cases. However, the proposed objectives in Opt 2 draw 54.2% less current compared to the objectives in Opt 1. The proposed objectives draw 10.4% less prime mover torque. When comparing the average source current per

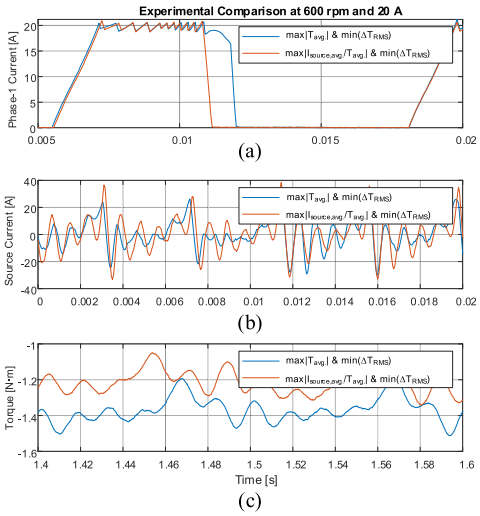

FIGURE 19. Experimental results at 600 r/min and 20 A current reference. (a) Phase current. (b) Source current. (c) Shaft torque.

TABLE 7. Comparison of Opt 1 and Opt 2 optimization objectives at 600 r/min and 20 A.

600 r/min at 20 A_{ref}	Opt 1 $\max\lvert T_{avg}\rvert$ & $\min(\Delta T_{RMS})$	Opt 2 $\max\lvert I_{source,avg}/T_{avg}\rvert$ & $\min(\Delta T_{RMS})$	% Change
Phase current RMS	8.62 A	7.35 A	14.7 %
Avg. source current	0.48 A	0.22 A	54.2 %
Avg. torque	-1.35 N·m	-1.21 N·m	10.4 %
Avg. source current per avg. torque	-0.35 A/N·m	-0.18 A/N·m	48.6 %

average torque for the two different objectives, the proposed optimization shows a 48.6% improvement.

C. EXPERIMENTAL VALIDATION OF OPTIMIZATION OBJECTIVES WITH 72 V SUPPLY VOLTAGE AND 2600 R/MIN

The speed is increased to 2600 r/min with a current reference of 20 A at the nominal dc-link voltage of 72 V. In Fig. 20(a), the proposed objectives in Opt 2 have a delayed turn-ON and earlier turn-OFF conduction angle which leads to shorter conduction interval when compared to the objectives in Opt 1. In both cases, the same source current oscillation frequency is observed, but the proposed objectives slightly increase the peak source current magnitude returned to the supply as shown in Fig. 20(b). The proposed objectives in Opt 2 greatly reduce the amount of prime mover torque as observed in Fig. 20(c). As shown in Table 8, the smaller conduction period with Opt 2 results in a 6.1% reduction in phase RMS current. The Opt 2 objectives result in 1.1% more source current generated when compared to the Opt 1 objectives. The proposed objectives result in the average generating torque to reduce by 9.7% when compared to Opt 1, which leads to an 11.8% increase in the amount of average source current per average torque.

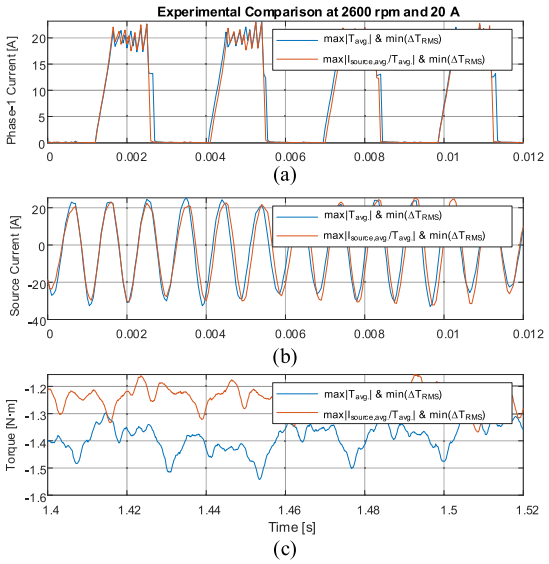

FIGURE 20. Experimental results at 2600 r/min and 20 A current reference. (a) Phase current. (b) Source current. (c) Shaft torque.

TABLE 8. Comparison of Opt 1 and Opt 2 optimization objectives 2600 r/min and 20 A

2600 r/min at 20 A_{ref}	Opt 1 $\max\lvert T_{avg}\rvert$ & $\min(\Delta T_{RMS})$	Opt 2 $\max\lvert I_{source,avg}/T_{avg}\rvert$ & $\min(\Delta T_{RMS})$	% Change
Phase current RMS	8.31 A	7.81 A	6.1 %
Avg. source current	-1.80 A	-1.82 A	1.1 %
Avg. torque	-1.38 N·m	-1.25 N·m	9.7 %
Avg. source current per avg. torque	1.30 A/N·m	1.46 A/N·m	11.8 %

VI. CONCLUSION

In this article, generating mode specific optimization objectives are developed for conduction angle control. The new objectives are determined using an exhaustive conduction angle search. Based on the exhaustive search results, new optimization objectives are proposed specific to generating mode to maximize the source current per average torque $\max\lvert I_{\text{source,avg}}/T_{\text{avg}}\rvert$ and minimize the torque ripple $\min(\Delta T_{\text{RMS}})$. An experimental setup is developed to validate the proposed method. The static flux linkage and torque characteristics of the motor have been characterized and the simulation models have been verified with experimental results. The experimental results show that the proposed generating-mode-specific objectives improve the average source current per average torque by 11.8% at 2600 r/min. The proposed method also reduced the RMS value of phase current by 6.1% for the same operating point, which can lead to lower copper loss. The proposed objectives improve the source current supplied to the source and reduce the phase current. Besides, the proposed optimization objectives result in a Pareto front which produces working conditions with less variation for all rotor speeds and current references.

ACKNOWLEDGMENT

The authors would like to thank Altair for their support with Flux, Compose, and Activate software, and MathWorks for their support with MATLAB and Simulink in this research.

REFERENCES

[1] "Energy Fact Book 2020-2021," Natural Resource Canada, 2020. Accessed: Oct. 2021. [Online]. Available: https://natural-resources.canada.ca/sites/nrcan/files/energy/energy_fact/energy-factbook-2020-2021-English.pdf

[2] B. Bilgin et al., "Making the case for electrified transportation," *IEEE Trans. Transp. Electrific.*, vol. 1, no. 1, pp. 4–17, Jun. 2015.

[3] D. Bauer, D. Diamond, J. Li, D. Sandalow, P. Telleen, and B. Wanner, "U.S. department of energy critical materials strategy," U.S. Dept. Energy Office Sci. Tech. Inf., Dec. 2010. Accessed: Nov. 2021. [Online]. Available: https://www.energy.gov/sites/prod/files/2019/06/f63/DOE_CMS2011_FINAL_Full_1.pdf

[4] "Mineral commodity summaries 2021," U.S. Geological Survey, 2021. Accessed: Dec. 2021. [Online]. Available: https://pubs.usgs.gov/periodicals/mcs2021/mcs2021.pdf

[5] "Rare earth elements: A review of production, processing, recycling, and associated environmental issues," United States Environmental Protection Agency, Dec. 2012. Accessed: Nov. 2021. [Online]. Available: https://nepis.epa.gov/Adobe/PDF/P100EUBC.pdf

[6] B. Bilgin and A. Emadi, "Electric motors in electrified transportation: A step toward achieving a sustainable and highly efficient transportation system," *IEEE Power Electron. Mag.*, vol. 1, no. 2, pp. 10–17, Jun. 2014.

[7] R. Tarvirdilu-Asl, S. Nalakath, B. Bilgin, and A. Emadi, "A finite control set model predictive torque control for switched reluctance motor drives with adaptive turn-off angle," in *Proc. IEEE Annu. Conf. Ind. Electron. Soc.*, 2019, pp. 840–845.

[8] Z. Xia, B. Bilgin, S. Nalakath, and A. Emadi, "A new torque sharing function method for switched reluctance machines with lower current tracking error," *IEEE Trans. Ind. Electron.*, vol. 68, no. 11, pp. 10612–10622, Nov. 2021.

[9] J. Liu, L. Wang, L. Yi, G. Zhu, and X. Yin, "Optimization of SRM direct instantaneous torque control strategy based on improved firefly algorithm," in *Proc. IEEE Conf. Energy Internet Energy Syst. Integr.*, 2019, pp. 364–368.

[10] N. Saha, S. Panda, and D. K. Sahoo, "Modified whale optimization technique for combined objective of torque ripple minimization and speed control of SRM drive," in *Proc. Int. Conf. Energy, Power Environ., Towards Clean Energy Technol.*, 2021, pp. 1–5.

[11] J. Deskur, T. Pajchrowski, and K. Zawirski, "Optimal control of current commutation of high speed SRM drive," in *Proc. Int. Power Electron. Motion Control Conf.*, 2008, pp. 1204–1208.

[12] A. Shahabi, A. Rashidi, and S. M. Saghaian-Nejad, "Torque ripple reduction of SRM drives below the base speed using commutation angles control," in *Proc. Iranian Conf. Elect. Eng.*, 2013, pp. 1–6.

[13] X. D. Xue et al., "Optimal control method of motoring operation for SRM drives in electric vehicles," *IEEE Trans. Veh. Technol.*, vol. 59, no. 3, pp. 1191–1204, Mar. 2010.

[14] M. K. Jha, N. Seth, N. Tyagi, and S. A. Khan, "SRM torque ripple reduction using grey wolf and teaching and learning based optimization in hysteresis control," in *Proc. IEEE Int. Conf. Intell. Technol.*, 2021, pp. 1–7.

[15] Y. Wang, H. Wu, W. Zhang, and Y. Ma, "A high efficiency direct instantaneous torque control of SRM using commutation angles control," in *Proc. IEEE Int. Conf. Elect. Mach. Syst.*, 2014, pp. 2863–2866.

[16] M. M. Namazi, M. M. Borujeni, A. Rashidi, S. M. S. Nejad, and J. W. Ahn, "Torque ripple reduction of switched reluctance motor drive with adaptive sliding mode control and particle swarm optimization," in *Proc. IEEE Int. Conf. Adv. Intell. Mechatron.*, 2015, pp. 371–376.

[17] M. Yaich and M. Ghariani, "Artificial intelligence-based control for torque ripple minimization in switched reluctance motor drives," in *Proc. IEEE Int. Conf. Sci. Techn. Autom. Control Comput. Eng.*, 2017, pp. 320–327.

[18] M. Zine, A. Chemsa, C. Labiod, M. Ikhlef, K. Srairi, and M. Benbouzid, "Coupled indirect torque control and maximum power point tracking technique for optimal performance of 12/8 switched reluctance generator-based wind turbines," *MDPI Mach.*, vol. 10, no. 11, Nov. 2022, Art. no. 1046.

[19] Y. Dou, Q. Wang, H. Chen, and D. Yu, "High efficiency control of switched reluctance generator above base speed," in *Proc. IEEE Int. Conf. Power Electron., Drives Energy Syst.*, 2016, pp. 1–6.

[20] A. Verma, S. S. Ahmad, and G. Narayanan, "Optimal switching angles for single-pulse-operated switched reluctance generator," in *Proc. Nat. Power Electron. Conf.*, 2021, pp. 1–6.

[21] Z. Yueying, Y. Chuantian, and Z. Chengwen, "Multi-objective optimization of switched reluctance generator for electric vehicles," in *Proc. 21st Int. Conf. Elect. Mach. Syst.*, 2018, pp. 1903–1907.

[22] B. Bilgin, J. W. Jiang, and A. Emadi, *Switched Reluctance Motor Drives: Fundamentals to Applications*. Boca Raton, FL, USA: CRC Press, 2018, pp. 189–192.

[23] B. Bilgin, A. Emadi, and M. Krishnamurthy, "Switched reluctance generator with higher number of rotor poles than stator poles," in *Proc. IEEE Transp. Electrific. Conf. Expo*, 2012, pp. 1–6.

[24] M. V. Terzic, H. Li, B. Bilgin, and A. Emadi, "Comparison of experimental methods for electromagnetic characterization of switched reluctance motors," in *Proc. IEEE Int. Conf. Elect. Mach.*, 2018, pp. 1881–1888.